JUSTC

Article

http://justc.ustc.edu.cn

Received: March 22, 2022; Accepted: May 09, 2022

Design and optimization of transparent scattering solar concentrator based on SiO_2 aerogel

Feng Zhang[1], Jun Bao[1], and Chen Gao[1,2] ✉

[1]*National Synchrotron Radiation Laboratory & Collaborative Innovation Center of Chemistry for Energy Materials, University of Science and Technology of China, Hefei 230029, China;*
[2]*School of Physical Sciences, University of Chinese Academy of Sciences, Beijing 100049, China*

✉Correspondence: Chen Gao, E-mail: cgao@ustc.edu.cn

Graphical abstract

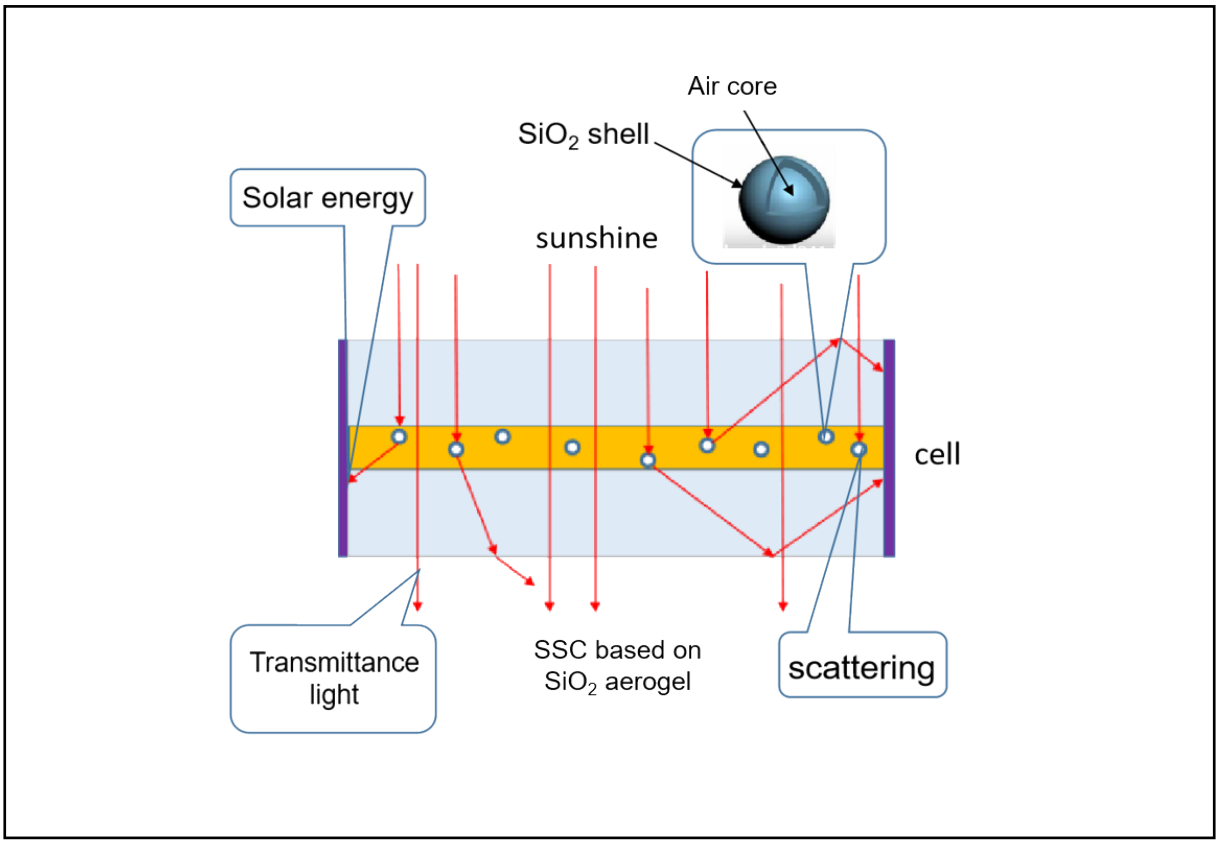

Structure of SSC based on SiO_2 aerogel.

Public summary

- Scattering solar concentrators based on SiO_2 aerogel were fabricated, which have excellent optical performance and moderate photoelectric performance.
- A Monte Carlo ray tracing program was developed and the multiple scattering mechanism that damages the efficiency was analyzed.
- An anisotropic scattering device was proposed to suppress the damage of the multiple scattering.

Citation: Zhang F, Bao J, Gao C. Design and optimization of transparent scattering solar concentrator based on SiO_2 aerogel. *JUSTC*, **2022**, 52(10): 2. DOI: 10.52396/JUSTC-2022-0047

JUSTC

Article

http://justc.ustc.edu.cn

Received: March 22, 2022; Accepted: May 09, 2022

Design and optimization of transparent scattering solar concentrator based on SiO_2 aerogel

Feng Zhang[1], Jun Bao[1], and Chen Gao[1,2] ✉

[1]*National Synchrotron Radiation Laboratory & Collaborative Innovation Center of Chemistry for Energy Materials, University of Science and Technology of China, Hefei 230029, China;*
[2]*School of Physical Sciences, University of Chinese Academy of Sciences, Beijing 100049, China*

✉Correspondence: Chen Gao, E-mail: cgao@ustc.edu.cn

Cite This: *JUSTC*, **2022**, 52(10): 2 (8pp)

Read Online

Abstract: Scattering solar concentrators (SSCs), an important component of transparent/translucent photovoltaic devices, can concentrate large-area sunlight on small-area solar cells while allowing some sunlight to pass through the devices. However, owing to the lack of suitable scattering materials, there have been few reports on SSCs in recent years. In this study, we fabricated SiO_2 aerogel-based SSCs and tested their performances. The photoelectric performance was found to be moderate. Additionally, the results demonstrated excellent transmittance and color rendering index, which meet the lighting requirements of the windows. A Monte Carlo ray tracing program was developed to simulate an SSC and analyze the fate of all photons. We also analyzed the multiple scattering mechanism in SSCs that damages the photoelectric efficiency of a device via theoretical simulation. Finally, we proposed an anisotropic scattering device that can increase the primary scattering and suppress multiple scattering, resulting in excellent photoelectric efficiency.

Keywords: solar concentrators; scattering; Monte Carlo ray tracing; aerogel

CLC number: TK513.1 **Document code:** A

1 Introduction

With further increases in the global energy crisis and pollution problems, solar energy has attracted increasing attention as an abundant and clean renewable energy source[1–5]. With the introduction of building integration photovoltaics (BIPV), the demand for transparent/translucent photovoltaic devices is increasing[6]. A solar concentrator, which constitutes a transparent waveguide with fluorescent material or scattering particles dispersed within and solar cells attached to the sidewalls of the waveguide, can perfectly meet this requirement[7].

When sunlight is directed toward the transparent waveguide, some of the photons will be absorbed by the fluorescent material or scattered by the scattering particle, and the reemitted or scattered light is transmitted in all directions. Because the refractive index of the waveguide is higher than that of air, total reflection occurs at the waveguide/air interface. Therefore, a part of the reemitted or scattered light is trapped inside the waveguide until a solar cell is attached to the sidewall. Thus, transparent/translucent photovoltaic devices can be achieved.

To date, only organic dyes[8–10] and quantum dots[11–13] have been successfully used as fluorescent materials and TiO_2 nanodots as scattering particles. Luminescent solar concentrators (LSCs) suffer from durability and efficiency issues owing to their limited lifetime and efficiency.

The scattering solar concentrator (SSC) was first demonstrated by Chau et al. in 2010[14]. As the scattering effect strongly depends on the refraction difference between the scattering particle and the waveguide, high-refraction materials, such as TiO_2 (n = 2.55), were selected as scatterers while the waveguide matrix was polymethyl methacrylate (PMMA, n = 1.49). Since then, few studies have been reported on SSCs, which may be due to the limited available material[15, 16]. Therefore, aerogels may be a suitable scattering material.

An aerogel is a low-density material foam, first reported by Kistle in 1931[17]. At the micro level, aerogel particles have a nano core-shell structure with a thin solid shell and an air core. Aerogels can be made from a variety of materials such as silica, carbon, and various oxides. For the SiO_2 aerogel, the refractive index of the shell is almost the same as that of optical waveguide materials such as glass, PMMA, and ethylene-vinyl acetate copolymer (EVA), which helps the outside shell to readily merge with the waveguide optically. The difference in the refractive index between the air core and shell is 0.5. Although this is smaller than that between TiO_2 and PMMA, it is already sufficiently large to cause significant scattering. In addition, the microscopic closed structure of the aerogel particles prevents the inside air from macroscopic convection, which improves the thermal insulation of the doped waveguide. According to these advantages, SSCs are an excellent choice.

In this paper, a nano SiO_2 aerogel (n = 1.0) was chosen as the scattering particle. Compared with TiO_2-based SSCs, aerogel-based SSCs have comparable efficiency while possessing the advantages of light weight and heat insulation, which are also critical characteristics for BIPV applications. We fabricated a series of nano SiO_2 aerogel-based SSCs and

DOI: 10.52396/JUSTC-2022-0047
JUSTC, **2022**, 52(10): 2

measured their efficiency and transparency as a function of the aerogel doping concentration. Moreover, we developed a Monte Carlo simulation program to trace the trajectory of an individual photon, similar to Refs. [18−20]. Through statistical analysis of the fate of a large number of randomly incident photons, the effects influencing the efficiency of the SSC were identified, and cascade scattering was found to be predominant. An anisotropic scattering SSC was proposed to further improve the efficiency.

2 Experiments

2.1 Aerogel

Our SiO_2 aerogel brick was purchased from Xiamen Nameite New Materials Technology Co., Ltd., and SiO_2 aerogel powder was obtained by ultrasonicating the brick in water for 30 min. The density of the aerogel was approximately 30 kg/m^3 and its porosity was above 90%. Fig. 1 shows a TEM image of the aerogel. We observed that most aerogel particles had spherical or polyhedral shapes. The size of the internal air core was 20–50 nm. Because the porosity was above 90%, the shell thickness was approximately 1/10 of the aircoresize.Wecandeducethatthethicknessoftheoutershellwas2–5 nm.

2.2 Fabrication of aerogel-based SSC

Amounts of 0.05, 0.1, 0.2, and 0.4 g of SiO_2 aerogel powder were weighed using an electronic balance and added into a beaker containing 30 mL of toluene solvent. The powder was dispersed in solvent using an ultrasonic cleaner for half an hour. Then, 50 g of EVA was added to the beaker, and the beaker was placed in a 70 ℃ stirring heater to allow sufficient dissolution of the EVA and mixing with the aerogel. Finally, uniform SiO_2 aerogel-dispersed EVA sol with mass concentrations of 0.1%, 0.2%, 0.4%, and 0.8% were obtained, and according to the densities of the SiO_2 aerogel (30 kg/m^3) and EVA (948 kg/m^3), the corresponding volume fractions are 2.9%, 5.8%, 11.2%, and 20.2%, respectively.

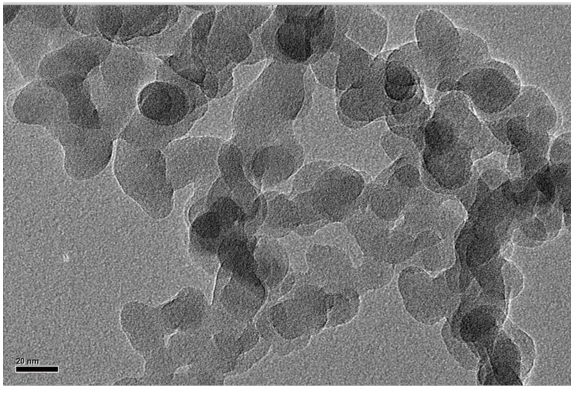

Fig. 1. TEM photograph of SiO_2 aerogel.

The sol was poured into a petri dish and placed in a vacuum oven to remove any residual solvent. The dried sol was tableted into a 2 mm thick EVA film using a flat vulcanizer. Two ultra-white glasses of 100 mm × 100 mm × 4 mm were ultrasonically cleaned with acetone and deionized water in sequence and then placed in a vacuum drying oven before use. The film was cut into pieces of 100 mm × 100 mm and sandwiched between two 4 mm thick ultra-white glasses of the same size (refractive index of 1.53). Then, the laminated glass was placed into a vacuum laminator at 110 ℃ for 20 min.

The solar cells used were single-crystal silicon solar cells purchased from Zhejiang Aiko Solar Energy Technology Co., Ltd.. The efficiency of the cell was approximately 17%, and each was cut to the size of 100 mm × 10 mm via laser cutting. Circuit boards of the same size were attached to protect the cells. Welding strips were welded onto the cells as electrodes. Four crystal silicon solar cells with the size of 100 mm × 10 mm were attached to the four edges of the laminated glass using a UV adhesive (refractive index of 1.49) to form the final SSC device. The four cells were connected in series to form an electrical output. Fig. 2a depicts the structure of the SSC and Fig. 2b presents a photograph of the SSC.

2.3 Cost

The main materials used in this device include ultra-white glass, EVA, solar cells, circuit boards, aerogels, welding trips, and UV glue. The welding trip and UV glue were only used in small amounts, and the cost is negligible. The prices of the ultra-white glass, aerogel, EVA, and solar cell (100 mm × 10 mm) were approximately ¥100 per square meter, ¥1000 per kilogram, ¥30 per kilogram, ¥1 per piece (including the cell cutting cost, the cell with size of 125 mm × 125 mm was ¥5 per piece), respectively. The circuit board was ¥0.5 for each

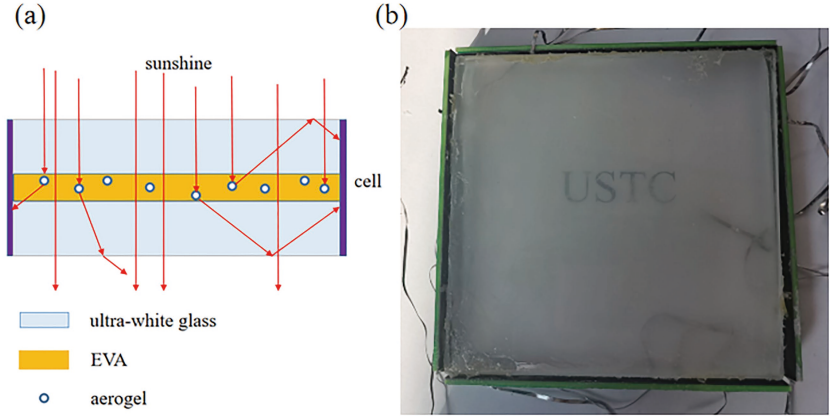

Fig. 2. (a) Structure of SSC; (b) photograph of 20.2% aerogel SSC.

DOI: 10.52396/JUSTC-2022-0047
JUSTC, **2022**, 52(10): 2

piece. Therefore, the total cost of a single device (100 mm × 100 mm) is

$$0.5\times4+4\times1+100\times2\times0.01+(30\times0.05+1000\times0.0004)=¥9.9. \quad (1)$$

As the process matures, the circuit board can be cancelled, and the cost of cell cutting decreases. The final cost of a single device is expected to be controlled within ¥5.

3 Results and discussion

3.1 Efficiency and transmittance

Fig. 3 shows the efficiency and transmittance of the SSCs as a function of the volume fraction of the SiO_2 aerogel. As the size of our SSCs exceeded the uniform region of the AM1.5 solar simulator, the efficiency was measured using a relative method. A Si solar cell was first calibrated under the AM1.5 solar simulator, and then the *I-V* curves of the solar cell and the SSCs were recorded with a Keithley 2400 digital source meter under the same sunshine. Efficiency was deduced from the ratio of the output. Fig. 4 displays the transmitted spectrum of a 20.2% SSC under sunshine measured using a portable spectrometer (EVERINE Company). Plots include the spectrum of sunlight measured under the same conditions, as well as the deduced transmitted spectrum.

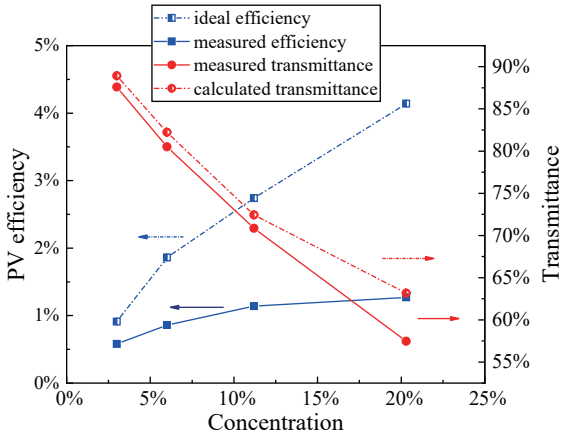

Fig. 3. Measured and calculated efficiencies and transmittances as functions of SiO_2 aerogel concentration.

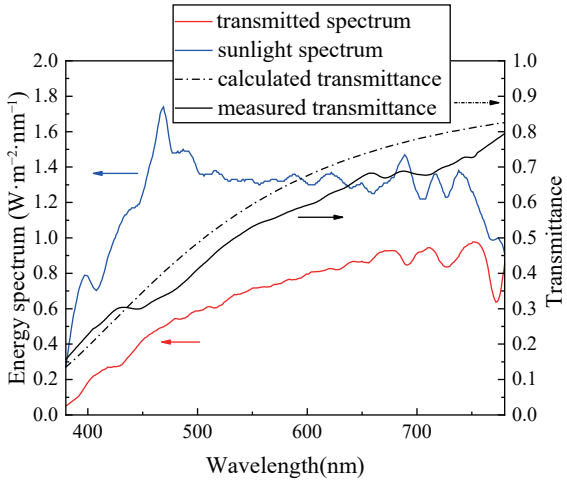

Fig. 4. Transmitted light intensity spectrum (red line) of a 20.2% aerogel SSC measured under sunshine, sunlight spectrum (blue line), and the measured (black line) and calculated (dash-dotted line) transmittance spectra.

It can be seen from Fig. 3 that the efficiency gradually increases with an increase in the volume fraction, while the transmittance decreases with an increase in the volume fraction. As the volume fraction increases from 2.9% to 20.2%, the efficiency increases from 0.58% to 1.27%, whereas the transmittance decreases from 89% to 57%. This is mainly because the higher the concentration, the more photons are scattered to the edges and converted into electrical energy. Consequently, fewer photons are transmitted to the SSCs. In addition to the transmitted photons and the photons reaching the cells, there is still some photon loss, which is probably because some photons leave the SSC through multiple scattering. The multiple scattering loss mechanism of the cone escape is discussed below.

This result can be explained by the Rayleigh scattering theory. As the diameter of the SiO_2 aerogel particles is approximately 20–50 nm, which is much smaller than the wavelength of sunlight, the transmittance can be calculated as[21]:

$$I = I_0\exp\left[\frac{3V_p x r^3}{4\lambda^4}\left(\frac{n_p}{n_m}-1\right)\right], \quad (2)$$

where I_0 is the incident intensity, x is the thickness of the EVA film, V_p is the volume fraction of the aerogel, r is the particle radius, λ is the wavelength of light, and n_p and n_m are the refractive indices of the aerogel particles and the transparent matrix, respectively.

The calculated transmittance and efficiency as functions of concentration are plotted in Fig. 3. It was found that the calculated transmittance is consistent with the measured one, while the calculated efficiency was much higher than the measured counterpart. The difference in efficiency is mainly because of the cascaded scattering. The effect of the cascaded scattering will be discussed in the following chapter.

3.2 Color rendering

Color rendering is a critical parameter in window or skylight applications. The color rendering index (CRI) of sunlight filtered by an SSC of 20.2% aerogel concentration is shown in Fig. 5, where almost all color rendering indexes (R1–R15) changed less after filtering, while the general color rendering index value Ra was as high as 97. The correlated color temperature (CCT) for sunlight filtered by the SSC was 4800 K. Thus, when using the SSC, no color distortion occurred and a comfortable color temperature range was obtained, as defined by Debije et al.[22]. For comparison, the CRI and CCT of sunlight filtered by a RED305 LSC were 60 and 3100 K, respectively, hence the SSC had good prospects compared with LSC in applications such as windows and skylights, among others.

3.3 Monte Carlo simulation

To further understand the optical process, a Monte Carlo simulation program was developed to trace the trajectory of photons inside the SSC. A flowchart of the program is presented in Fig. 6, similar to Ref. [18]. First, a photon with random

DOI: 10.52396/JUSTC-2022-0047
JUSTC, **2022**, 52(10): 2

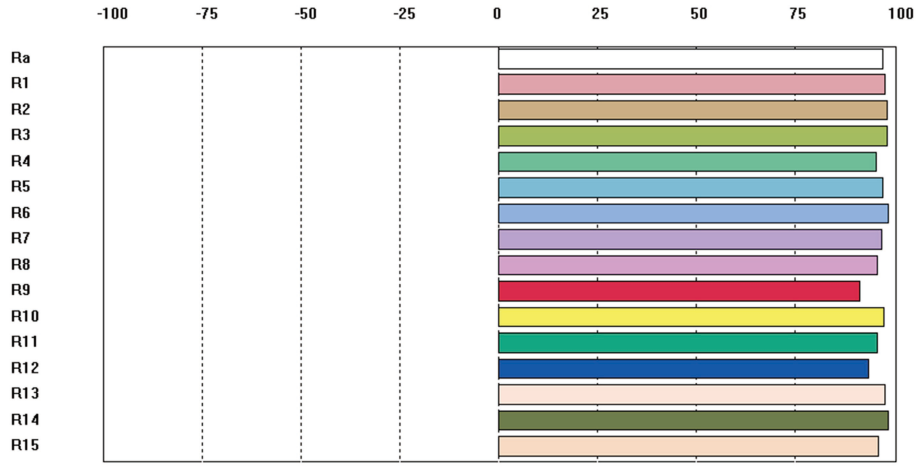

Fig. 5. Color rendering index (Ra) and monochromatic color rendering index (R1–R15) of the SSC (20.2%).

wavelength and position was launched. Thus, it has probability p to be scattered by the aerogel particles according to the aerogel concentration, which can be calculated by Eq.(3):

$$p = 1 - \exp\left[\frac{3V_{\mathrm{p}}xr^3}{4\lambda^4}\left(\frac{n_{\mathrm{p}}}{n_{\mathrm{m}}} - 1\right)\right]. \tag{3}$$

It is worth noting that the nanoparticles agglomerated, but during processing, the microcosmic structure of the aerogels was not destroyed, and the air core and SiO_2 shell structures remained. Each nanoparticle couls still be regarded as an air core (20–50 nm, refractive index = 1)-SiO_2 shell (refractive index = 1.5)-EVA (refractive index = 1.5) or other aerogel shell (refractive index = 1.5) structures from inside to outside. Therefore, in the calculations and simulations, the data were reasonable.

The unscattered photons were transmitted to the device. In contrast to the situation in the LSC, where the re-emitted photons show an isotropic distribution, the scattering demonstrated an anisotropic angular distribution. For spherical particles that were far smaller than the wavelength, the distributions were peanut and dumbbell shaped for the s- and p-polarization components, respectively (Fig. 7).

Therefore, the angular distribution probability of scattered photons can be calculated by Eq.(4):

$$P(\theta) = \frac{1}{2}(1 + \cos^2(\theta)). \tag{4}$$

Accordingly, the direction of the scattered photons was determined from a distribution with a random number. From this direction, it was determined whether the photon would undergo total internal reflection. However, photons propagating inside the waveguide may be scattered again by the aerogel particles, i.e., multiple scattering. The scattering probability and direction were calculated in the same manner. This process was repeated until the photon either reached the waveguide edge or escaped from the waveguide. After 500000 photon fates were obtained, the transmission spectrum and efficiency were obtained.

Fig. 8 presents the AM1.5 and simulated transmission spectra of the 20.2% aerogel SSC.

Fig. 9 shows the fate statistics of 500000 simulated photons for a 20.2% aerogel SSC. From the figure, we observe that 71% of the photons transmitted the SSC without scattering. There were 6.4% of photons that reached the cells attached to the waveguide edges. Among the scattered photons, 18.6% of the photons escaped the waveguide owing to the small incident angle, and most of them came from the multiple-scattering effect. Therefore, the efficiency estimated from single-scattering theory (Eq.(1)) was much larger than the measured value (see Fig. 3). The photons leaving the bottom of the SSC

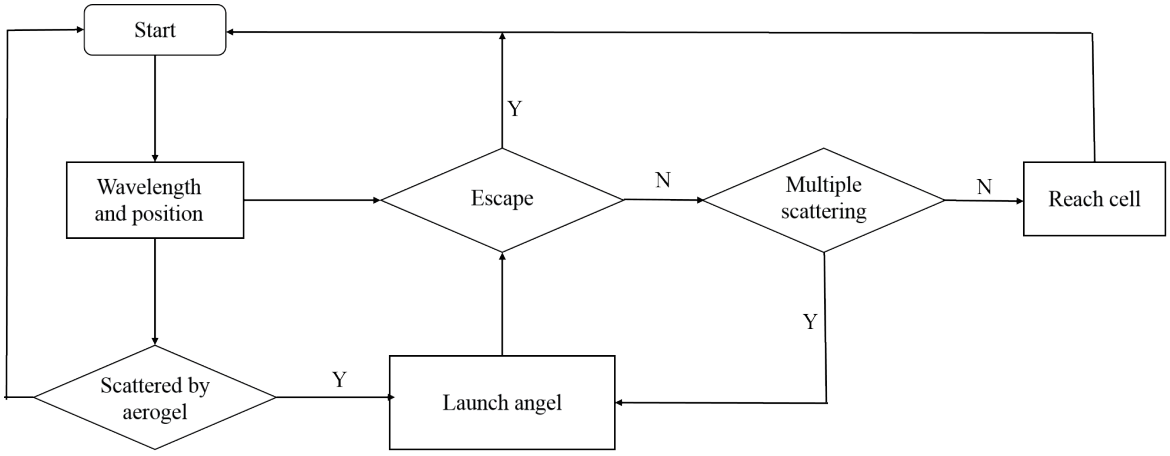

Fig. 6. Monte Carlo ray-tracing program flowchart.

DOI: 10.52396/JUSTC-2022-0047
JUSTC, **2022**, 52(10): 2

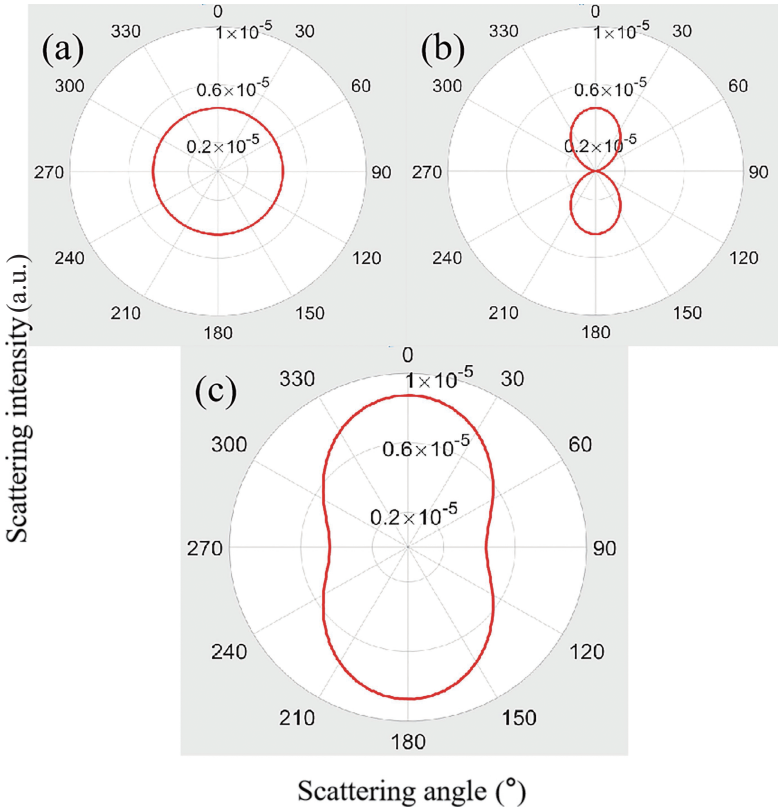

Fig. 7. (a) Angular distribution of s-polarized light scattering; (b) angular distribution of p-polarized light scattering; (c) total angular distribution of natural light scattering.

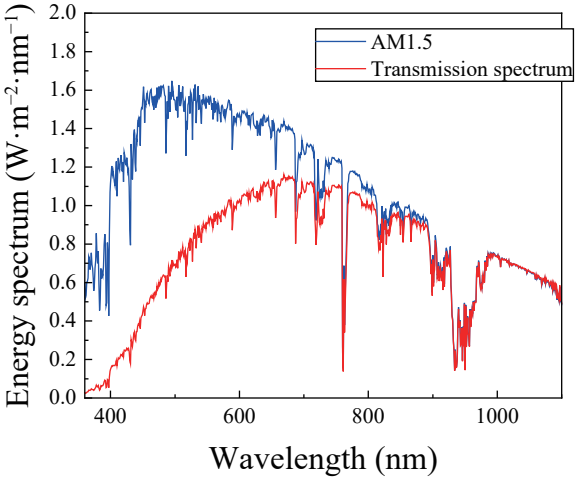

Fig. 8. AM1.5 and simulated transmission spectra of SSC (20.2%).

were approximately 80%, which included all the unscattered photons and half of the escaping photons. The corresponding energy transmittance was 70%, which was slightly larger than the transmittance measured by the portable spectrometer (57%). The portable spectrometer had a small acceptance one-half angle, whereas the refraction angle of most escaping photons was large, so that some escaping photons were not detected by the portable spectrometer. The simulation considering multiple scattering yielded 0.52%, 0.81%, 1.1%, and 1.4% efficiencies for the 2.9%, 5.8%, 11.2%, and 20.2% aerogel SSCs, respectively, coinciding with the experiment effectively.

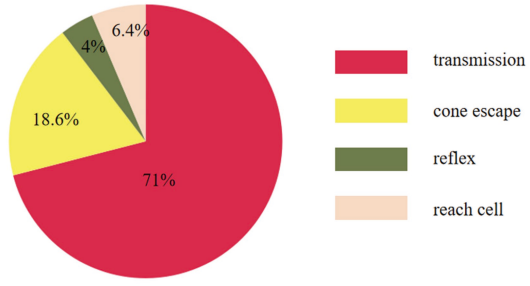

Fig. 9. Fate statistics of the 500000 simulated photons.

Multiple scattering also caused unequal contributions toward the efficiency of the SSC surface. Fig. 10 shows the typical simulated distribution of the photon collection probability (defined as the ratio of collected photons to scattered photons) for our device with size of 100 mm × 100 mm × 10 mm, and 20.2% volume concentration. It was found that the incident photon near the central position has a small chance of being collected by the solar cells attached to the edge, compared with those photons incident near the edges. This is because the scattered photon near the center has to travel a long path to reach the edge; on the path, it could be scattered again and has a large chance of escaping the waveguide. Regarding this, an efficiency comparison should be performed at the same surface area because a small SSC usually exhibits a larger efficiency than a large SSC. The same conclusion is also true for LSC, where self-absorption plays a role similar to that of multiple scattering in SSC[23].

DOI: 10.52396/JUSTC-2022-0047
JUSTC, **2022**, 52(10): 2

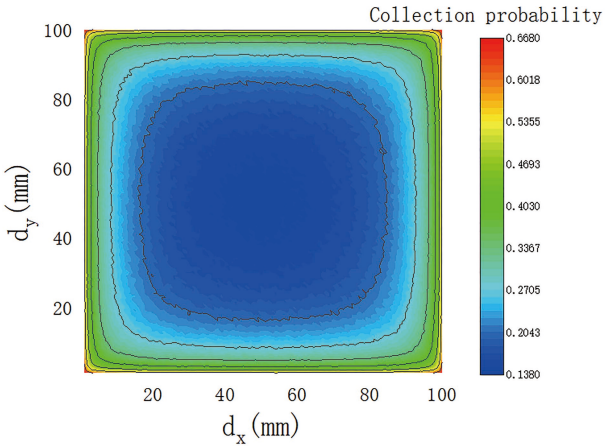

Fig. 10. Simulated collection probability of a 100 mm × 100 mm SSC surface (20.2%).

3.4 Anisotropic scattering

As discussed above, multiple scattering causes photons to escape from waveguides. As a typical sample, the collection probability (Fig. 10) of a scattered photon decreases from 60% near the edge to 13% at the center. This effect limits the expansion of SSC size, which is considered one of the most important advantages of SSC.

To minimize this effect, we proposed the use of anisotropic particles such as nanosheets as the scattering medium. As shown in Fig. 11, if such nanoparticles can be arranged in a parallel manner, the propagating photon will encounter a small intersection, whereas the incident photon will still encounter a normal intersection. Consequently, the incident photon has almost the same probability of being scattered into a propagating photon, and the propagating photon has a small probability of being re-scattered into escaping photons.

To quantitatively elucidate this idea, the finite-difference time-domain (FDTD) method was used to calculate the scattering intensity of photons, and the results are shown in Fig. 12.

The scattering intensities of photons incident perpendicular to the nanosheets (blue line), parallel to the nanosheets (red line), and at a 30° angle to the nanosheets (orange line) are shown in Fig. 12. The scattering intensity of photons parallel to the nanosheets was only 1/3 that of photons perpendicular to the nanosheets, and the scattering intensity of photons incident to the nanosphere was larger than the scattering intensity of photons incident parallel to the nanosheets and smaller than the scattering intensity of photons incident perpendicular to the nanosheets; thus, the scattered photons trapped in the SSC experienced less re-scattering and reached

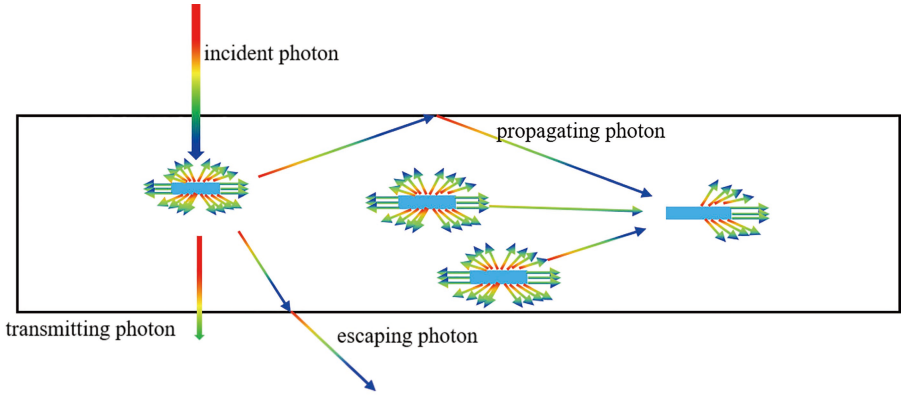

Fig. 11. Schematic of the anisotropic scattering of parallel arranged nanosheets.

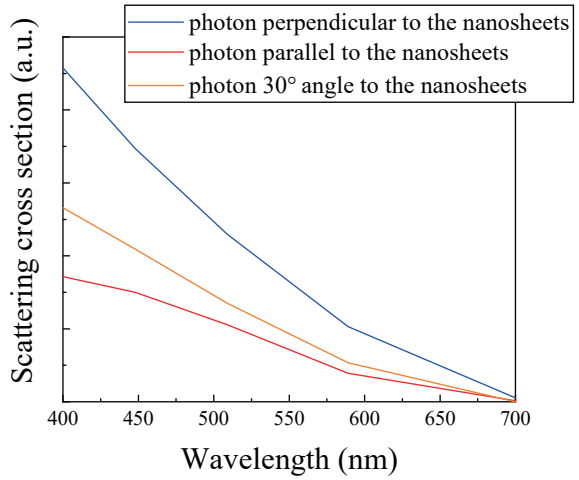

Fig. 12. Scattering intensity of incident photons. Nanosheet size: 200 nm in diameter, 20 nm in height. Waveguide matrix refractive: 1.5, nanosheet refractive: 2.55.

the cell more easily. The angular distributions of the scattering probability are depicted in Fig.13a–c. The distributions were strong in the forward and backward directions, weak in the lateral direction, and similar to that of spherical particles (Fig. 13d).

A similar Monte Carlo ray-tracing simulation, as described in the above section, was also performed for this anisotropic scattering nanosheet doped into an SSC with size of 100 mm × 100 mm × 10 mm and volume concentration of 2%. Here, the index (2.55) of TiO_2 was used in the simulation. Fig. 14 displays the fates of 500000 photons undergoing anisotropic scattering. It was found that 22% of the photons reached the attached cells. Compared with 6.8% isotropic scattering, anisotropic scattering demonstrated approximately three times the gain in the photon collector, and the corresponding efficiency was expected to reach 4.4%.

4 Conclusions

SiO_2 aerogel-based scattering concentrating devices were

DOI: 10.52396/JUSTC-2022-0047
JUSTC, **2022**, 52(10): 2

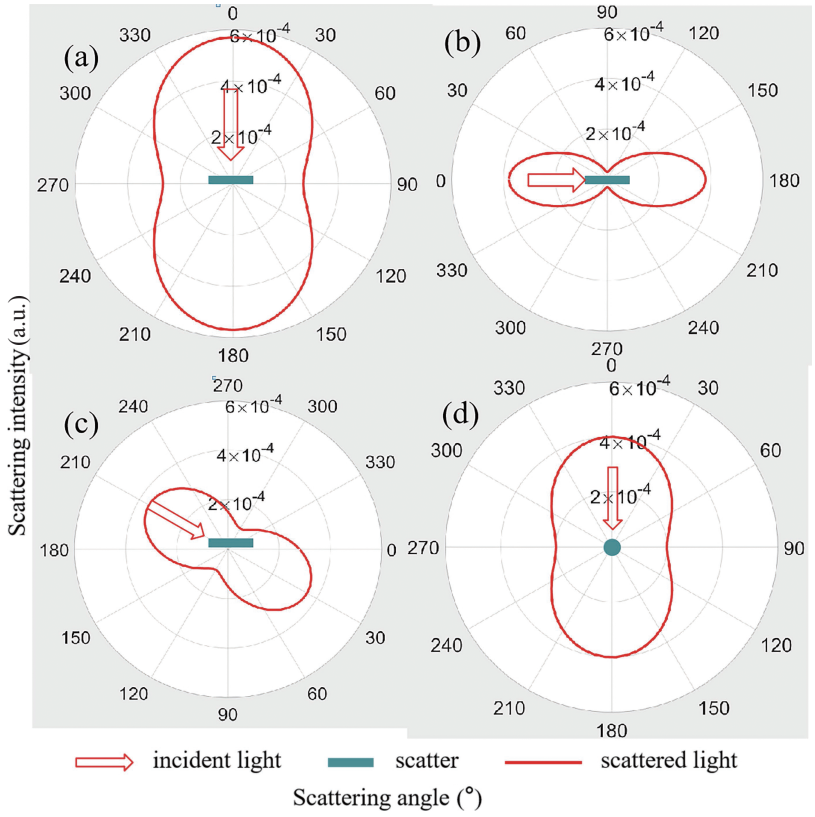

Fig. 13. Typical angular distributions of scattering probability for photons incident (a) perpendicular, (b) parallel, and (c) 30° to the nanosheets and (d) perpendicular to the nanosphere (radius = 50 nm).

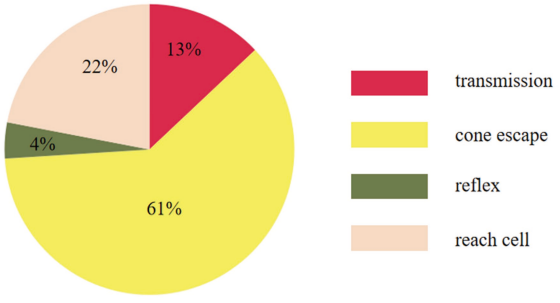

Fig. 14. Fate statistics of the 500000 photons under nanosheet SSC.

fabricated, and the related photovoltaic and light transmission properties were analyzed based on the experimental results. It was found that its photoelectric efficiency could reach 1.27% and its transmittance reached 57%, while the CRI of the device was still as high as 97%. Owing to its low cost and good heat insulation properties, this device can be used in building-integrated photovoltaics. Further, using Monte Carlo simulation, we found that multiple scattering loss is the dominant cause of low efficiency. To overcome this shortcoming, anisotropic scattering was proposed, and it was found that aligned nanosheets can effectively improve primary scattering and reduce multiple scattering by the FDTD method. The Monte Carlo simulation also demonstrated that the anisotropic scattering device can achieve the ideal efficiency of 4.4%. The study reveals the principle and characteristics of SSC, and the excellent performance of SiO_2 aerogel SSC proves that it will become an important branch of transparent/translucent photovoltaic devices. The anisotropic scattering device even gave better performance expectations than most LSCs. The follow-up work will be devoted to the improvement of the preparation process of SiO_2 aerogel SSC and the experimental preparation of anisotropic scattering devices, so as to further move towards industrialization.

Acknowledgements

This work was supported by the Chinese Universities Scientific Fund (CX3430000001).

Conflict of interest

The authors declare that they have no conflict of interest.

Biographies

Feng Zhang is a Ph.D. student at the University of Science and Technology of China. His research interests focus on luminescent solar concentrator.

Chen Gao received his Ph.D. degree from the University of Science and Technology of China (USTC) in 1990. He worked as a Professor at USTC from 1999 to 2019. He joined the faculty of the University of Chinese Academy of Sciences in 2019. His research interests include the optical system and solar energy.

References

[1] Papakonstantinou I, Portnoi M, Debije M G. The hidden potential of luminescent solar concentrators. *Advanced Energy Materials*, **2021**,

DOI: 10.52396/JUSTC-2022-0047
JUSTC, **2022**, 52(10): 2

11 (3): 2002883.

[2] Bauhuis G J, Mulder P, Haverkamp E J, et al. 26.1% thin-film GaAs solar cell using epitaxial lift-off. *Solar Energy Materials and Solar Cells,* **2009**, *93* (9): 1488–1491.

[3] Chae Y T, Kim J, Park H, et al. Building energy performance evaluation of building integrated photovoltaic (BIPV) window with semi-transparent solar cells. *Applied Energy,* **2014**, *129*: 217–227.

[4] Zhang J, Wang M, Zhang Y, et al. Optimization of large-size glass laminated luminescent solar concentrators. *Solar Energy,* **2015**, *117*: 260–267.

[5] Whalley L D, Frost J M, Jung Y K, et al. Perspective: Theory and simulation of hybrid halide perovskites. *The Journal of Chemical Physics,* **2017**, *146* (22): 220901.

[6] Miyazaki T, Akisawa A, Kashiwagi T. The effects of solar chimneys on thermal load mitigation of office buildings under the Japanese climate. *Renewable Energy,* **2006**, *31* (7): 987–1010.

[7] Debije M G, Verbunt P P C. Thirty years of luminescent solar concentrator research: Solar energy for the built environment. *Advanced Energy Materials,* **2012**, *2* (1): 12–35.

[8] Currie M J, Mapel J K, Heidel T D, et al. High-efficiency organic solar concentrators for photovoltaics. *Science,* **2008**, *321* (5886): 226–228.

[9] Debije M G. Solar energy collectors with tunable transmission. *Advanced Functional Materials,* **2010**, *20* (9): 1498–1502.

[10] Zhang Y, Sun S, Kang R, et al. Polymethylmethacrylate-based luminescent solar concentrators with bottom-mounted solar cells. *Energy Conversion and Management,* **2015**, *95*: 187–192.

[11] Meinardi F, McDaniel H, Carulli F, et al. Highly efficient large-area colourless luminescent solar concentrators using heavy-metal-free colloidal quantum dots. *Nature Nanotechnology,* **2015**, *10* (10): 878–885.

[12] Meinardi F, Colombo A, Velizhanin K A, et al. Large-area luminescent solar concentrators based on 'Stokes-shift-engineered' nanocrystals in a mass-polymerized PMMA matrix. *Nature Photonics,* **2014**, *8* (5): 392–399.

[13] Wilton S R, Fetterman M R, Low J J, et al. Monte Carlo study of PbSe quantum dots as the fluorescent material in luminescent solar concentrators. *Optics Express,* **2014**, *22*: A35–A43.

[14] Chau J L H, Chen R T, Hwang G L, et al. Transparent solar cell window module. *Solar Energy Materials and Solar Cells,* **2010**, *94* (3): 588–591.

[15] Chen R T, Chau J L H, Hwang G L. Design and fabrication of diffusive solar cell window. *Renewable Energy,* **2012**, *40* (1): 24–28.

[16] Chen R T, Kang C C, Lin J F, et al. Optimal design for the diffusion plate with nanoparticles in a diffusive solar cell window by Mie scattering simulation. *International Journal of Photoenergy,* **2013**: 481637.

[17] Kistler S S. Coherent expanded aerogels and jellies. *Nature,* **1931**, *127* (3211): 741–741.

[18] Tummeltshammer C, Taylor A, Kenyon A J, et al. Losses in luminescent solar concentrators unveiled. *Solar Energy Materials and Solar Cells,* **2016**, *144*: 40–47.

[19] Tummeltshammer C, Taylor A, Kenyon A J, et al. Homeotropic alignment and Förster resonance energy transfer: The way to a brighter luminescent solar concentrator. *Journal of Applied Physics,* **2014**, *116* (17): 173103.

[20] Zhang F, Zhang N N, Zhang Y, et al. Theoretical simulation and analysis of large size BMP-LSC by 3D Monte Carlo ray tracing model. *Chinese Physics B,* **2017**, *26* (5): 054201.

[21] Novak B M. Hybrid nanocomposite materials—between inorganic glasses and organic polymers. *Advanced Materials,* **1993**, *5* (6): 422–433.

[22] Vossen F M, Aarts M P J, Debije M G. Visual performance of red luminescent solar concentrating windows in an office environment. *Energy and Buildings,* **2016**, *113*: 123–132.

[23] Tummeltshammer C, Brown M S, Taylor A, et al. Efficiency and loss mechanisms of plasmonic luminescent solar concentrators. *Optics Express,* **2013**, *21*: A735–A749.

DOI: 10.52396/JUSTC-2022-0047
JUSTC, **2022**, 52(10): 2